10th International Conference on Composite Science and Technology
ICCST/10
A.L. Araújo, J.R. Correia, C.M. Mota Soares, et al. (Editors)

IMPACT PERFORMANCE OF BIOMIMETIC HELICOIDAL COMPOSITE PLATES

Nigel H.H. Ngern[*], Jia Shun Shang[†], Vincent B.C. Tan[†]

[*] Department of Mechanical Engineering
National University of Singapore
Block EA #01-22
9 Engineering Drive 1
Singapore 117576
nigel.ngern@nus.edu.sg

[†] Department of Mechanical Engineering
National University of Singapore
Block EA #01-22
9 Engineering Drive 1
Singapore 117576
jiashun@u.nus.edu
mpetanbc@nus.edu.sg

Key words: Helicoidal, Biomimetic, Ballistic, Impact, Plate

Summary: *The helicoidal shell structure is found in the exoskeleton of the mantis shrimp, which is able to withstand high impact loads and velocities. Biomimetic plates with varying angular displacements between constituent unidirectional carbon-epoxy prepreg plies were fabricated and tested to determine the ballistic limit and its relationship with inter-ply angle, and the results are compared with a conventional cross-ply orientation. The helicoidal configuration yields a distinctly higher ballistic limit when the inter-ply angle is small, with a greater degree of delaminated area resulting in greater capacity for absorbing and distributing impact loads.*

1 INTRODUCTION

The peacock mantis shrimp is a crustacean with a fearsome reputation as a ferocious predator of the sea due to its unique hunting ability: it strikes its prey (crustaceans and molluscs) with a hammer-like appendage, generating up to 226 N of force[1] and an impact velocity of 23 m/s[2] in the process. One or two blows will cause fracture in the shell of prey, with dismemberment occurring occasionally.

During territorial disputes, it is known to effectively defend against blows from its own kind by utilising its tail segment (telson) to defend itself[3]. The telson is likely to be structured to withstand the same impact forces that are experienced by its prey, yet it can endure multiple repeated strikes. The same can be said for the hammer. While the hammer of

the peacock mantis shrimp has been the focus of several structural studies [1, 2, 4], the structure of the telson has, to date, received far less attention.

The structure of the telson cuticle (shell layer) is similar to the cuticles of the hammer as well as the shells of other crustaceans: it is primarily composed of microscopic chitin fibres that are arranged in layers embedded in a protein matrix[5, 6, 7]. Each layer has fibres running parallel to each other, and each layer is oriented with a very slight angular displacement to the adjacent one such that a spiralling effect is observed in the overall macrostructure. This helicoidal structure comprises tens of thousands of individual layers (Figure 1). To discern the mechanical performance of this helicoidal arrangement, a composite system based on biomimicry of the tail shell structure was created.

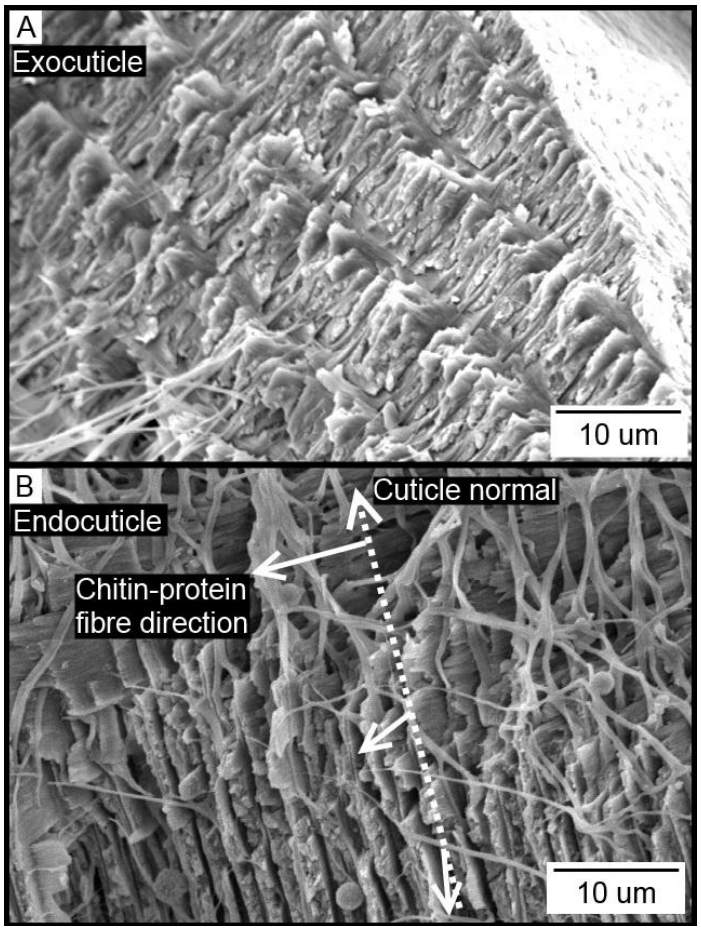

Figure 1: SEM images of (A) outer cuticle layer and (B) inner cuticle layer of the peacock mantis shrimp telson. The helicoidal orientation of the chitin-protein fibres can be observed.

2 SPECIMEN CREATION

In order to characterize the bio-inspired composite system proposed in the current study, it is important to utilize common engineering materials for composites. In the current study, the material used for the fabrication of specimens is unidirectional T700/2510 carbon-epoxy prepreg (CU-075, CGT International, Singapore). The physical properties of the material are summarised in Table 1.

Nominal thickness (mm)	Resin content (%)	Areal weight (g/m^2)		
		Carbon fibre	Resin	Total
0.08	38±2	75	46	121

Table 1: Physical properties of T700/2510 prepreg

Although the actual telson cuticle comprises tens of thousands of chitin-protein fibre layers with very minute angle change between them, the laminate configurations are designed such that they are composed of less than 40 layers in order to minimise uncertainty arising from fabrication defects as well as improper curing. Referencing from the work of Apichattrabrut and Ravi-Chandar [8], the ply rotation angle for the helicoidal specimens was decided at 10°. A structure with total angular displacement of 180° between the uppermost and bottom layers, termed a single helicoid (SH), would thus comprise 19 plies. A double helicoid (DH), with a total angular displacement of 360°, would contain 37 plies. In addition, a smaller ply rotation angle of 5° was introduced to investigate the effect of ply rotation angle on ballistic resistance after the results of the DH was analysed.

The performance of the helicoidal configuration is compared against the cross-ply configuration, which is a balanced and symmetric layup configuration commonly used in industry. A cross-ply can also be described as a helicoidal orientation with an inter-ply angle of 45°. The configurations used in the experiments are summarised in Table 2.

Designation	Description	No. of plies	Configuration
CP19	cross-ply	19	[(0°/90°)$_9$/0°]
CP37	cross-ply	37	[(0°/90°)$_{18}$/0°]
SH19	single helicoidal (10°)	19	[0°/-10°/…/-180°]
DH37	double helicoidal (10°)	37	[0°/-10°/…/-360°]
SH37	Single helicoidal (5°)	37	[0°/-5°/…/-180°]

Table 2: Summary of laminate configurations.

Prepreg pieces of dimension 100 mm by 100 mm are cut from the roll for the fabrication of laminates for the experiments. The laminates are cured using an autoclave system (Thermal Equipment Corporation, USA) programmed with a cure cycle according to the manufacturer's recommendation.

The shapes of the helicoidal and cross-ply specimens are essentially different. However, initial tests conducted on specimens trimmed to 100 mm in diameter showed that there is no difference in the response compared to the normal untrimmed specimens. In addition, trimming the specimens might introduce microscopic defects if performed without the utmost care. To reduce chances of random damage arising from the trimming operation, the tests were performed on untrimmed specimens.

3 BALLISTIC TEST

In order to evaluate the impact resistance of the helicoidal configuration, a series of ballistic experiments are conducted to obtain the ballistic limits for the SH19 and DH37 configurations. For comparison, CP19 and CP37 specimens are also tested. In light of the

performance of the DH37, SH37 specimens were subsequently created and tested later in the study.

3.1 Ballistic Test Procedure

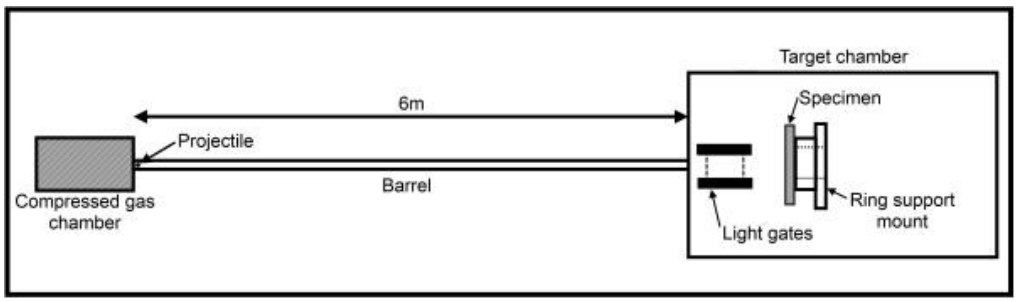

Figure 2: Schematic of ballistic test setup.

Figure 2 shows a schematic of the setup for the ballistic experiments. A smooth bore gas gun is used to propel a spherical steel projectile of diameter 12 mm and mass 6.90 g. The impact velocity of the projectile is measured using a pair of light gates positioned between the gas gun muzzle and the target. Specimens were mounted using low-strength adhesive putty (Bostik Blu Tack) on a solid metal ring with outer and inner diameters of 90 and 75 mm, respectively (Figure 3). This imposed a simply-supported boundary condition, as the adhesive used merely holds the specimen in place and does not bond it to the support. The centre of the specimen is aligned with the trajectory of the projectile.

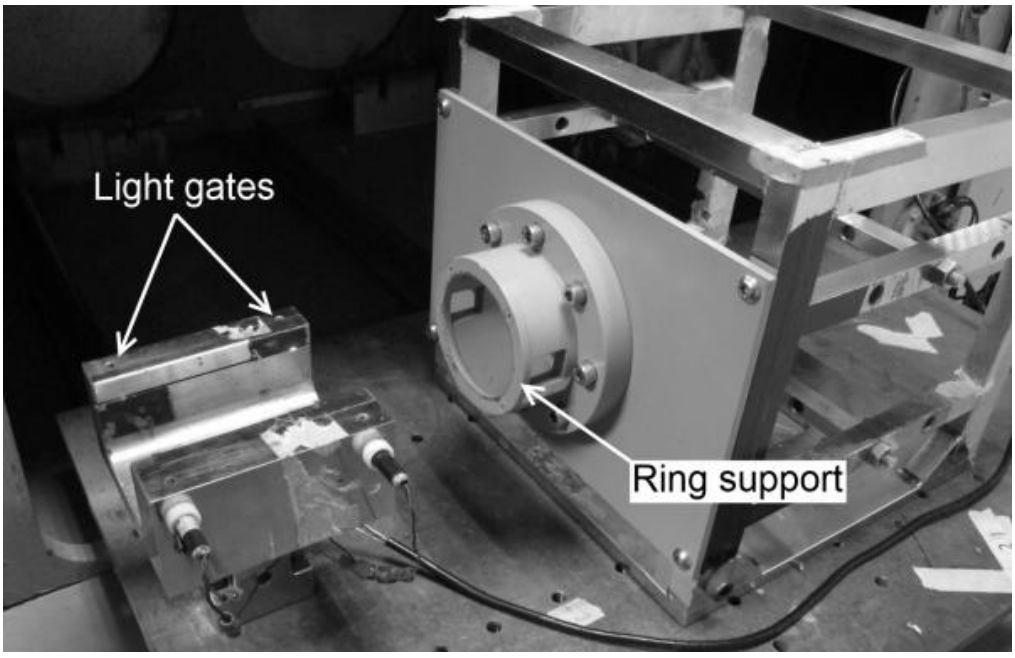

Figure 3: Setup within the target chamber showing ring support, sans specimen.

As the number of specimens is limited and thus insufficient for a statistical determination of ballistic limit according to standard test procedures (e.g. V_{50} in Mil-Std-662F and NIJ 0101.06 standards), an alternative method is adopted. In the current method, each test is

performed on a fresh specimen with increasing projectile velocity until the velocity at which the test specimen is perforated and the velocity at which the test specimen is not perforated differ by less than 5 m/s. The ballistic limit is then taken to be the average of the two values. Subsequently, the two specimens for each configuration are examined for damage.

3.2 Ballistic Test Results

Table 3.4 summarises ballistic limits for the various configurations. The ballistic limit for SH19 was 93.78 m/s, which was 32.9% lower than that of CP19 at 139.78 m/s. As for the 37-ply configurations, the ballistic limit for the DH37 was 142.70 m/s, which was marginally better (by 1.6%) than that of CP37. However, the ballistic limit of the SH37 was 9.7% higher than the CP37, at 154.10 m/s.

Configuration	Ballistic Limit (m/s)	% Difference
CP19	139.78	-
SH19	93.78	-32.9 (vs. CP19)
CP37	140.47	-
DH37	142.70	1.6 (vs. CP37)
SH37	154.10	9.7 (vs. CP37)

Table 3: Summary of ballistic limits for various laminate configurations.

Given that the 37-ply configurations are essentially two stacked 19-ply configurations, it is interesting to note that there was a 52.2% improvement in ballistic limit for DH37 over SH19, but there is no significant improvement for CP37 compared to CP19. Thus, doubling the thickness of the laminate only seemed to affect the helicoidal orientation. Another noteworthy observation is that a reduction in the inter-ply angle from 10 ° in the DH37 to 5 ° in the SH37 specimens yielded an increase in ballistic limit of 8%.

4 ANALYSIS OF SPECIMENS

For post-experiment damage analysis, specimens which encountered the lowest velocity where perforation occurred were selected. The specimens were subjected to a non-destructive CT scan, in order to obtain images of the internal damage. As the SH37 specimens were created and tested towards the end of the study, the representative specimen was not scanned and analysed in time for this report.

The scans are performed using the Skyscan 1076 (Skyscan, Belgium) micro-CT scanner at a resolution of 18 μm. The maximum width of specimens for the scanner is limited to 3 cm. Therefore prior to scanning, the specimens are cut to the allowable width using a diamond wafering saw along the 0 ° direction of the top ply, with 1.5 cm on each side of the specimen centre. Reconstruction of raw images is performed using the designated software NRecon (Skyscan, Belgium). Subsequently, images of cross-sections are extracted using Dataviewer (Skyscan, Belgium).

4.1 Damage in 19-ply Specimens

From Figure 4, the CP19 shows through-thickness cracks in the 0 ° and 90 ° directions within a localised region, due to a combined effect of matrix and fibre failure. Delamination occurs within this region. Conversely, the SH19 shows delamination occurring to a further extent from the impact point in a spiral fashion, due to the helicoidal structure (Figure 5). The extent of matrix and fibre failure in the CP19 specimen is greater than that of the SH19, possibly accounting for the higher observed ballistic limit.

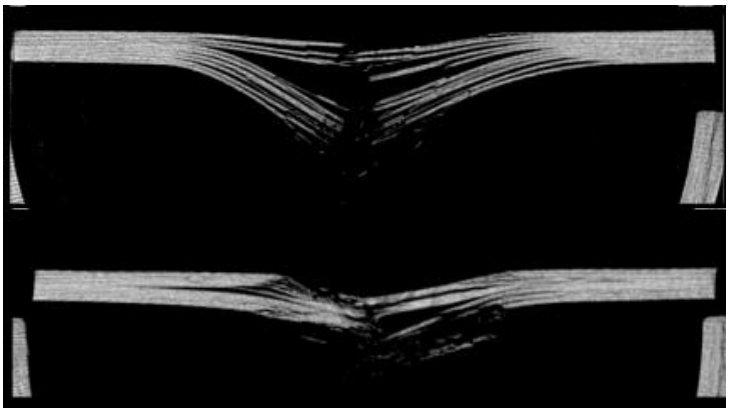

Figure 4: Micro-CT images of transverse sections of CP19 (top) and SH19 (bottom).

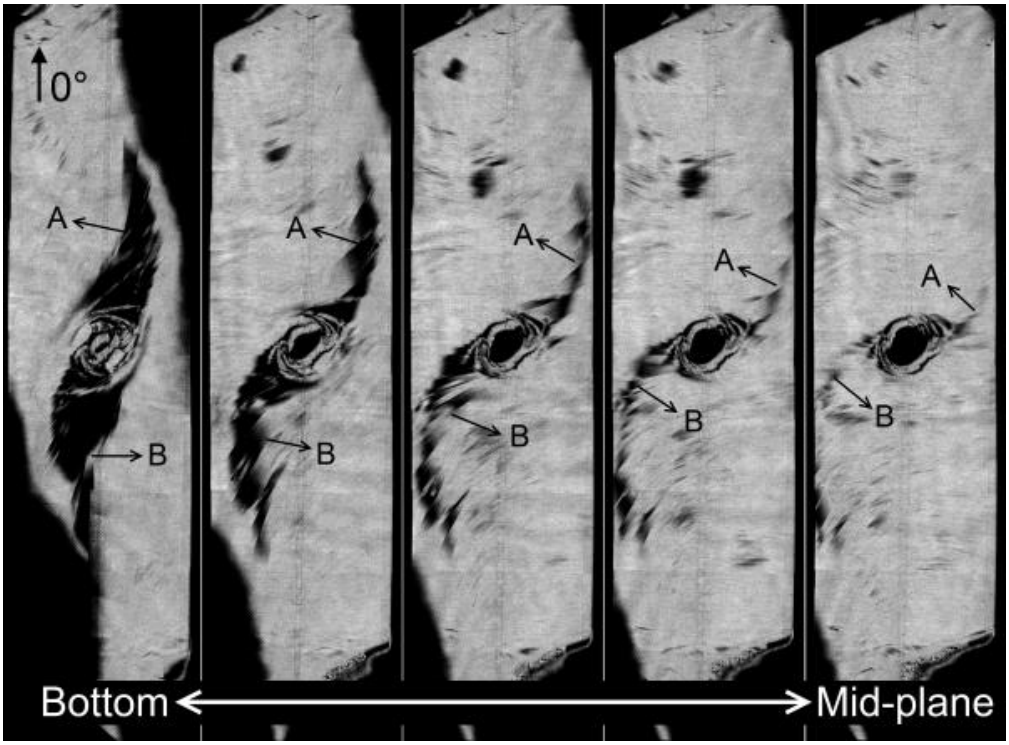

Figure 5: Micro-CT images of in-plane sections showing rotating path of delamination cracks (indicated by arrows) in SH19 specimen. Peripheral dark areas are due to twist of specimen geometry.

4.2 Damage in 37-ply Specimens

The types of damage in the 37-ply specimens are similar to those found in the 19-ply specimens. The CP37 showed an area comparable to the CP19 where the damage is localised. However, the DH37 now shows a greater extent of matrix and fibre failure compared to the CP37, in addition to a larger delamination crack that also spirals through the entire thickness of the specimen (Figure 6).

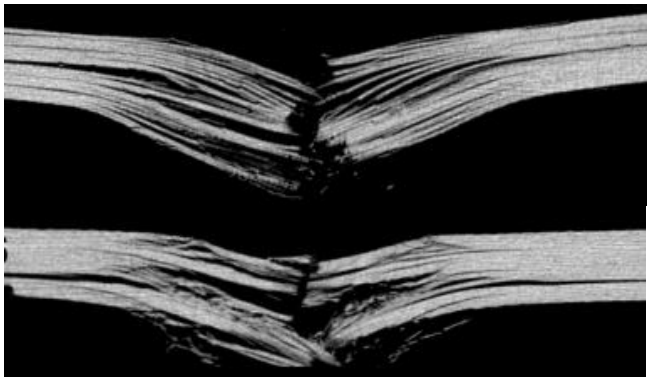

Figure 6: Micro-CT images of transverse sections of CP37 (top) and DH37 (bottom).

4.3 Comparison of Failure Mechanisms

Based on the aforementioned damage observed in the specimens, it can be concluded that the helicoidal and cross-ply configurations have distinctly different failure mechanisms. The dominant mode of damage in specimens with helicoidal configurations is delamination. In contrast, cross-ply specimens do not exhibit the same extent of delamination.

One possible explanation for the significant improvement in ballistic limit of DH37 over SH19 could be that there is more extensive delamination in the former since the overall ply rotation is also doubled. In comparison, damage in cross-ply specimens is localized in the centre regardless of the number of plies. Therefore the helicoidal configuration has the advantage of increased energy dissipation as the number of rotations increase. Hence it can be expected that having triple or more helicoidal rotations, the ballistic limit of the specimen will better than a cross-ply specimen with an equivalent number of plies.

In the helicoidal specimens, the reduction in angle between adjacent plies has drastically reduced in-plane fracture propagation[9]. This might also account for the SH37 having a higher ballistic limit as compared to the DH37, due to the smaller angle between the plies in the former.

5 CONCLUSIONS

This current research is an attempt to investigate the morphology of the mantis shrimp's telson cuticle and an attempt at biomimicry of this tail plate system resulted in a laminated carbon-epoxy composite system. Using SEM, the stacking arrangement of the chitin-protein layers was established to be of a helicoidal configuration. Apart from the bio-inspired composite system, a conventional composite layup commonly used in industry was tested

and used as a reference system against which the performance of the proposed design can be compared.

In the helicoidal configuration, the two key parameters are the ply rotation angle and number of helicoidal stacks in the laminate. Relative to the performance of the cross-ply configuration, if the ply rotation angle is reduced, the helicoidal laminate would reduce in-plane fractures within each ply. If the number of layers in the helicoidal configuration is increased, the helicoidal laminate would experience greater delamination as well as fibre failure. Both of these effects serve to increase the amount of impact energy being absorbed, yielding a higher ballistic limit. It seems that there is also a certain minimum number of layers required which, if exceeded, result in the helicoidal configuration outperforming the conventional cross-ply.

REFERENCES

[1] S.N. Patek, R.L. Caldwell, Extreme impact and cavitation forces of a biological hammer: strike forces of the peacock mantis shrimp Odontodactylus scyllarus. *Journal of Experimental Biology*, **208**, 3655-3664, 2005.
[2] S.N. Patek, W.L. Korff, R.L. Caldwell, Biomechanics: deadly strike mechanism of a mantis shrimp. *Nature*, **428**, 819-820, 2004.
[3] R.L. Caldwell, H. Dingle, Stomatopods. *Scientific American*, ***234***, 80-89, 1976.
[4] J.D. Currey, A. Nash, W. Bonfield, Calcified cuticle in the stomatopod smashing limb. *Journal of Materials Science*, **17**, 1939-1944, 1982.
[5] H. Fabritius, C. Sachs, D. Raabe, S. Nikolov, M. Fri ák, J. Neugebauer, Chitin in the exoskeletons of arthropoda: From ancient design to novel materials science. *Chitin*, Springer Netherlands, 35-60, 2011.
[6] A. C. Neville, Biology of the arthropod cuticle. *Springer*, 1975.
[7] A. C. Neville, Cuticle: organization. *Biology of the Integument*, J. Bereiter-Hahn, A. G. Matoltsy, & K. S. Richards, eds., Springer Berlin Heidelberg, 611-625, 1985.
[8] T. Apichattrabrut, K. Ravi-Chandar, Helicoidal composites. *Mechanics of Advanced Materials and Structures*, **13**, 61-76, 2006.
[9] J. Tao, C. T. Sun, Influence of ply orientation on delamination in composite laminates. *Journal of Composite Materials*, **32**, 1933-1947, 1998.